Optimal Control Allocation Strategy for an Energy-efficient PTC Heater-based Electric Vehicle Passenger Cabin Heating System

Luka Grden[1)*], Joško Deur[1)], Branimir Škugor[1)], and Ivan Cvok[2)]
[1)] University of Zagreb, Faculty of Mechanical Engineering and Naval Architecture, Zagreb, Croatia
e–mail: luka.grden@fsb.unizg.hr, josko.deur@fsb.unizg.hr, branimir.skugor@fsb.unizg.hr
[2)] Rimac Technology, Zagreb, Croatia
e–mail: ivan.cvok@rimac-technology.com

ABSTRACT

Electric vehicles (EVs) experience significant driving range degradation in low ambient temperature conditions, primarily due to the elevated energy demand of heating system. This paper proposes an optimal control strategy for a positive temperature coefficient (PTC) heater-based electric minibus heating system, which is aimed to exploit actuators' redundancy for energy consumption minimization and driving range extension. The strategy optimally allocates control inputs of multiple actuators to provide heating power demanded by a superimposed proportional-integral (PI) feedback controller of the passenger cabin air temperature. The optimal allocation maps prescribe coolant pump flow, blower air flow, and inlet air temperature references, and they are obtained by comprehensive simulations of a high-fidelity multi-physics heating system model over a wide range of quasi-stationary operating conditions. A low-level PI controller is further designed for the full, allocation-related range of operating points to track the allocated inlet air temperature reference, while commanding the PTC heater power. The overall control strategy is validated through co-simulation with a high-fidelity vehicle model in comparison with an industry baseline strategy, demonstrating a considerable energy consumption reduction in both quasi-stationary and transient (heat up) conditions, as well as improved control performance in terms of shorter heat up intervals.

KEYWORDS

Electric vehicle, cabin heating system, PTC heater, optimization, control allocation, energy efficiency

INTRODUCTION

Driving range reduction at extreme ambient temperatures remains one of the principal drawbacks of electric vehicles (EVs) [1]. This is because of increased battery electricity consumption by the vehicle heating, ventilation and conditioning (HVAC). EV cabin heating is conventionally provided by high-voltage positive temperature coefficient (PTC) heaters, as a simple and robust solution [2]. In addition to the heater itself, these systems generally employ auxiliary actuators such as blower fans and coolant pumps. The primary limitation of PTC heaters is that their coefficient of performance (COP) cannot exceed 1, i.e., 1 kWh of electrical energy is needed to generate 1 kWh of heating energy. To overcome this weakness, heat-pump systems have recently been introduced in EV cabin HVAC systems, which can achieve significantly higher COP values through exploiting the ambient heat and powertrain and battery

* Corresponding author

waste heat [3]. To operate efficiently, such multi-actuator systems require advanced control strategies capable of optimally coordinating multiple control actions [4].

A range of HVAC control approaches have been reported in literature. A rule-based proportional-integral-derivative (PID) controller is applied in [5] to conventional HVAC systems to regulate blower air flow in dependence on the calculated thermal load. The controller gains are scheduled by a neural network (NN) with respect to different ambient conditions. PID control is also considered in [2], where additional feed-forward action was used to reduce the effect of transport delay, commonly observed in coolant-to-air heating systems. More advanced strategies, such as hierarchical optimal control allocation, have been developed to coordinate multiple actuators of a heat-pump system in [6]. Here, an optimal allocation of actuators is executed with respect to the heating power demand, where the allocation maps are obtained via offline multi-objective genetic algorithm (GA) optimization, as detailed in [7]. Since the proposed approach assumes the quasi-stationary HVAC conditions, the strategy is suboptimal in abrupt transient conditions occurring for instance during the cabin heat-up period. Thus, the insights gained through globally-optimal offline control trajectory optimization is employed in [8] to modify the control allocation strategy towards improving its transient performance. Furthermore, online optimization control techniques are also used, typically through a model predictive control (MPC) framework [9], offering the improved performance and thermal comfort in both transient and quasi-stationary conditions [10], as well as the control system design flexibility, but at the cost of significant computational burden.

Although much of the literature emphasizes the benefits of heat-pump systems in EVs [11], the cost-effective PTC heating systems continue to be applied. The efficiency of heat pumps can be sensitive to ambient disturbances and deteriorates under very cold climate conditions, so that they are usually combined with a supplementary PTC heater anyway [12]. Moreover, as shown in [13], such hybrid architectures can operate more efficiently because of keeping the heat-pump compressor closer to its optimal operating region.

This paper modifies and extends the control allocation strategy applied previously to a heat-pump system [6] to a PTC heater-based system. Although structurally simpler, PTC systems also include multiple actuators that can be optimally coordinated to improve the energy efficiency and thermal comfort. The actuators coordinated include air blower, coolant pump and the PTC heater itself. The strategy is based on optimal allocation maps, which are derived through offline optimization for different cabin temperature and heat power demand operating points. The heat power demand is determined by a superimposed proportional-integral (PI) feedback controller. To tune the controller through numerical parameter optimization, a computationally fast, linear control-oriented model is identified based on the system high-fidelity model. The low-level PI controller of allocated cabin inlet air temperature outputs the PTC heater power, and it is optimized analytically for a simplified heating system model. The overall control system is verified through simulations based on the high-fidelity model, and the results are compared to those obtained through an industry baseline control strategy (mimicking the on-vehicle control strategy).

The remainder of this paper is structured as follows. Section I presents the high-fidelity thermal model used for control system design parametrization and verification. Section II introduces the hierarchical control framework, including the superimposed cabin air temperature controller, the control allocation strategy, and the low-level cabin inlet air temperature controller. The same section presents design of the three control subsystems. Section III

presents the simulation results and compares them with the industry baseline results. The main findings are summarized in Section IV.

HVAC AND CABIN SYSTEM

The paper deals with an electric minibus HVAC system operating solely in heating regime based on a PTC heater (an A/C, i.e. cooling functionality is provided by a separate unit and an additional fuel-power heater booster is not considered [14]). The HVAC system behaviour is represented by a high-fidelity, multi-physics simulation model implemented in the Dymola environment (Fig. 1, [14]). The system consists of three actuators: PTC heater, coolant pump and air blower fan associated with a radiator situated in the upper part of the cabin. The corresponding control inputs are the PTC heater power setpoint $P_{PTC,R}$, the coolant pump flow $\dot{V}_p$ and the volumetric blower fan air flow $\dot{V}_{bf}$. The relevant HVAC model outputs include the cabin heating core outlet/cabin inlet temperature T_{in}, the PTC heater outlet coolant temperature T_{clnt}, blower fan air mass flow rate $\dot{m}_{bf}$, and the corresponding actuator power consumptions P_{PTC}, P_p and P_{bf}. The respective power consumption of air blower fan and the coolant pump is approximated by operating point lookup tables based on the data in specification sheets.

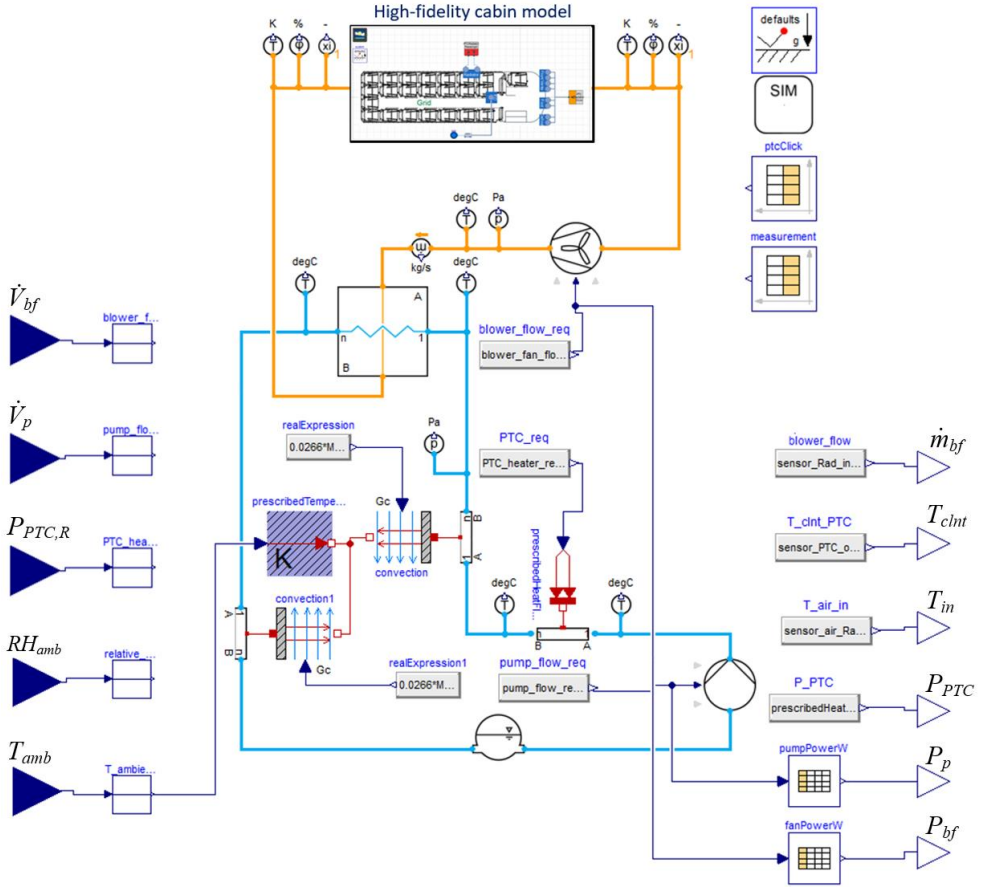

Figure 1. Vehicle heating system model implemented in Dymola environment [14]

The minibus passenger cabin is represented by a multi-zonal control volume moist air model. The cabin model consists of 45 volumes which captures the nonuniform cabin air temperature distribution. It is developed by using XRG Dymola Library and parameterized based on available experimental data obtained from measurements conducted at several seats for the external/ambient temperature T_{amb} = 0 °C (see [14] for more details). For the control strategy development, the air temperature at the middle of passenger cabin aisle is chosen as a representative temperature. To facilitate its use within the co-simulation loop, the high-fidelity

model has been exported as a Functional Mock-up Unit (FMU) block and subsequently imported into MATLAB Simulink, where the control strategy is implemented.

CONTROL SYSTEM DESIGN

Overall structure of control system

The proposed hierarchical control system is described by the structural block diagram in Fig. 2. The control strategy consists of (i) a superimposed PI cabin temperature controller that outputs the heating power demand $\dot{Q}_{h,R}$, (ii) optimal control allocation maps that coordinate the individual actuators, and (iii) a low-level cabin inlet air temperature PI controller that commands the PTC heater power. Based on the demanded heating power $\dot{Q}_{h,R}$ and the cabin temperature T_{cab}, the control allocation determines the air blower fan and coolant pump volume flow commands, $\dot{V}_{bf}$ and $\dot{V}_p$, respectively, as well as the inlet air temperature reference $T_{in,R}$. The blower fan and pump inputs are applied directly to the corresponding actuators (open-loop control), while $T_{in,R}$ is fed to the low-level feedback controller. The ambient condition disturbance vector **d** includes the ambient temperature and the vehicle velocity, which are in this paper set to constant values of 0 °C and 50 km/h, respectively. To limit the coolant temperature in the absence of explicit/cascaded coolant temperature controller, a P controller-like safety mechanism.

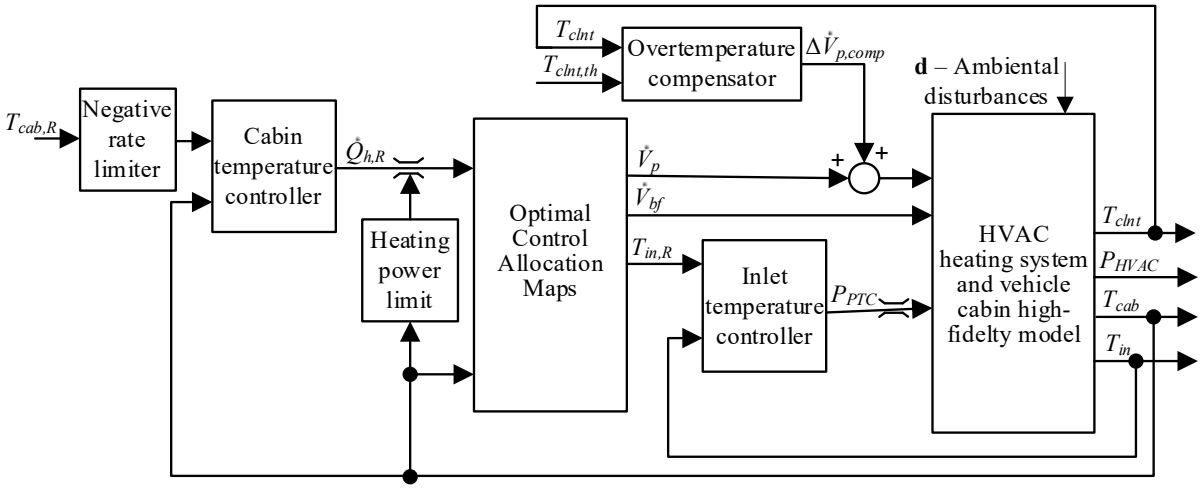

Figure 2. Structural block diagram of hierarchical minibus heating control system, with high-fidelity process model represented by Fig. 1

Optimal control allocation maps

Generating simulation dataset. The optimal control allocation maps transform the heating power demand $\dot{Q}_{h,R}$ and the lumped cabin air temperature T_{cab} to low-level controller inputs. Since the T_{cab} dynamics are slow relative to the controlled HVAC inputs and the associated heating power output, the relatively detailed and complex cabin thermal dynamics model (see upper portion of Fig. 1) can be excluded from the allocation maps optimization, i.e., a computationally-efficient instantaneous optimization procedure is applied based on constant boundary conditions for T_{cab} (and RH_{cab}) [6]. It should be noted that such a control allocation approach ensures optimal control only in quasi-steady state conditions, i.e., where the inlet air temperature T_{in} temperature is relatively close to its reference $T_{in,R}$. During pronounced transients, such as the initial system heat-up, the inlet temperature T_{in} can significantly differ from the reference $T_{in,R}$, thus leading to generally sub-optimal control allocation. Nevertheless,

quasi-steady-state conditions dominate over sufficiently long driving periods, resulting in overall nearly optimal system behaviour.

To derive the optimal allocation maps, a grid-search optimization method has been employed. Firstly, extensive automated simulations were performed by using the high-fidelity HVAC model, with enough time (in this case, $t_{sim} = 2000$s) left for the system to reach stationary conditions. The relevant HVAC outputs include the total power consumption P_{HVAC}, the inlet air temperature T_{in}, the coolant temperature T_{clnt} and the respective heating power $\dot{Q}_h$, defined by Eq. (2), which are saved for the grid-search algorithm. The simulation were performed for a wide range of operating points, including different combinations of air temperature boundary conditions T_{cab}, PTC heater power P_{PTC}, and air blower fan and coolant pump flows, $\dot{V}_{bf}$ and $\dot{V}_p$, respectively, over a relatively dense grid (Table 1). Actuator hardware limits are imposed by setting the corresponding control input ranges for simulations, as depicted in Table 1.

Table 1. Control input simulation grid

Actuator grid resolution and imposed limits
$P_{PTC} = \{500 : 250 : 5000\}$ W
$\dot{V}_{bf} = \{50 : 50 : 250\}$ m^3/h
$\dot{V}_p = \{2 : 2 : 30\}$ L/min

Optimization. Once the overall simulation dataset is prepared, the grid-search algorithm (see Algorithm 1 below) is used to identify the optimal actuator combinations that minimize the total power consumption:

$$J = \min(P_{HVAC}) = \min\left(P_{PTC} + P_{bf} + P_p\right), \quad (1)$$

for the given heating power demand $\dot{Q}_{h,R}$ given by (c_p = specific heat capacity, ρ_{cab} = cabin air density):

$$\dot{Q}_h = c_p \rho_{cab} \dot{V}_{bf} (T_{in} - T_{cab}) \quad (2)$$

While accounting for the following operational constraints:

$$\begin{gathered} 30°\text{C} \leq T_{in} \leq 60°\text{C}, \\ T_{clnt} \leq 90°\text{C}. \end{gathered} \quad (3)$$

The algorithm consists of two search phases for each operating/allocation point. In the first phase, linear interpolations of T_{in}, T_{clnt}, $\dot{Q}_h$, and P_{HVAC} are constructed, to enhance optimization efficiency and accuracy. A high-resolution grid (80x80 equally spaced points) of operating points $(\dot{V}_{p,grid}, \dot{V}_{bf,grid})$ is defined (finer than in Table 1). For each grid point, the corresponding P_{PTC} required to achieve the target $\dot{Q}_{hR}$ is determined. Each candidate triple $\left(\dot{V}_p, \dot{V}_{bf}, P_{PTC}\right)$ is then checked against operational constraints (4), and a feasible point yielding the minimum total power P_{HVAC} (see Eq. (2)) is stored as the optimal result. If no feasible point exists, which typically occurs when $\dot{Q}_{h,R}$ is outside the system limits, the solutions are discarded, and a second, fallback routine is activated. In this second phase, the total power minimization is not performed, but instead the heat output $\dot{Q}_h$ is maximized to approach the prescribed $\dot{Q}_{h,R}$ as closely as possible, while satisfying the operational constraints. For the defined operating points $(T_{cab}, \dot{Q}_{hR})$ (see Fig. 2), Fig. 3 describes the achieved HVAC heating power outputs $\dot{Q}_h$ with respect to prescribed target $\dot{Q}_{hR}$, which clearly indicates the HVAC operational limit curves, used in Fig. 2 to properly limit the superimposed controller. Along

with the above-described cabin temperature-dependent upper limit, a constant lower heating power limit (set to 1000 W) is set to satisfy the lower constraint of Eq. (3) (see Algorithm 1).

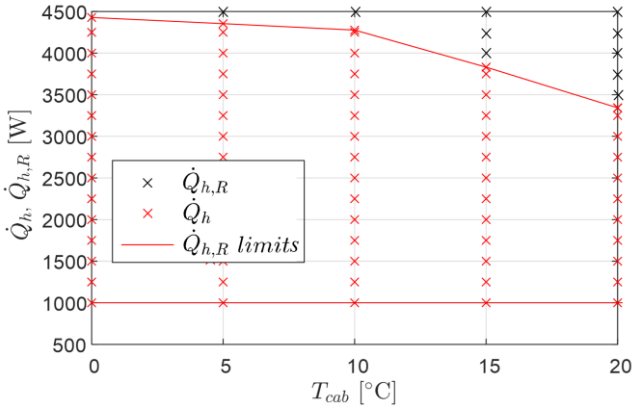

Figure 3. Illustration of determining HVAC system heating power limits in dependence on cabin temperature

Algorithm 1. Grid-search algorithm

FOR each cabin temperature $T_{cab} \in \{0, 5, 10, 15, 20\}$ °C :

- From filtered dataset build linear interpolant functions of output allocation variables:

$$f_{\dot{Q}_h}(\dot{V}_p, \dot{V}_{bf}, P_{PTC}), f_{P_{tot}}(\dot{V}_p, \dot{V}_{bf}, P_{PTC}), f_{T_{in}}(\dot{V}_p, \dot{V}_{bf}, P_{PTC}), f_{T_{clnt}}(\dot{V}_p, \dot{V}_{bf}, P_{PTC})$$

FOR each target heating level $\dot{Q}_{h,R} \in \{1000, 1250, 1500, \dots, 4500\}$ W:

P^*_{HVAC} = Inf // Initializing optimal/minimal power consumption

FOR each point in $(\dot{V}_{p,grid}, \dot{V}_{bf,grid})$:

- Find P_{PTC} that minimises $|f_{\dot{Q}_h}(\dot{V}_p, \dot{V}_{bf}, P_{PTC}) - \dot{Q}_{hR}|$
- Check if point $(\dot{V}_p, \dot{V}_{bf}, P_{PTC})$ satisfies:
  - $P_{PTC,\min} \leq P_{PTC} \leq P_{PTC,\max}$
  - $T_{in,\min} \leq f_{T_{in}}(\dot{V}_p, \dot{V}_{bf}, P_{PTC}) \leq T_{in,\max}$
  - $f_{T_{clnt}}(\dot{V}_p, \dot{V}_{bf}, P_{PTC}) \leq T_{clnt,\max}$
- IF point satisfies constraints AND $P_{HVAC} < P^*_{HVAC}$:
  - $P^*_{HVAC} = P_{HVAC}$
  - Store $(\dot{V}_p, \dot{V}_{bf}, P_{PTC})$

IF no feasible point is found: // Find feasible one which provides $\dot{Q}_h$ as close as possible to $\dot{Q}_{hR}$

$\Delta\dot{Q}^*_{hR}$ = Inf // Initialization

FOR each point in $(\dot{V}_{p,grid}, \dot{V}_{bf,grid})$:

FOR P_{PTC} grid

- Check feasibility
  - $T_{in,min} \leq f_{T_{in}}(\dot{V}_p, \dot{V}_{bf}, P_{PTC}) \leq T_{in,max}$
  - $f_{T_{clnt}}(\dot{V}_p, \dot{V}_{bf}, P_{PTC}) \leq T_{clnt,max}$
- Evaluate $\Delta\dot{Q}_h = |f_{\dot{Q}_h}(\dot{V}_p, \dot{V}_{bf}, P_{PTC}) - \dot{Q}_{hR}|$
- IF point is feasible AND $\Delta\dot{Q}_h < \Delta\dot{Q}^*_{hR}$
  - $\Delta\dot{Q}^*_{hR} = \Delta\dot{Q}_{hR}$
  - Store $(\dot{V}_p, \dot{V}_{bf}, P_{PTC})$

Control allocation maps. The obtained optimal allocation maps are shown in Fig. 5 for the considered range of $\dot{Q}_{h,R}$ and T_{cab}. The operating points are spaced at equidistant 250 W intervals over heating power reference, except of the last operating point determined by the system's heat output limit (highlighted in yellow in Fig. 5). As shown in Fig. 5c, the PTC heater power P_{PTC} rises linearly with the heating power demand $\dot{Q}_{h,R}$, and its allocation is relatively insensitive to on cabin temperature. Figs. 5d and 5e shows the resulting coolant and cabin inlet air temperatures, T_{clnt} and T_{in}, which are within the prescribed limits (cf. Eq. (1)). At lower values of T_{cab}, T_{in} is mostly saturated at its lower limit and it reaches the upper limit only in the highest heating power demand points. Fig. 5b indicates that the air blower fan flow $\dot{V}_{bf}$ is generally allocated toward the higher end of the operating range, where in the case of highest T_{cab} it is allocated on full flow rate almost over the whole range of heating power demands. To maintain the commanded $\dot{Q}_{hR}$ when T_{in} is saturated at the lower limit, the air blower fan flow increases linearly, and once it reaches the upper limit, T_{in} rises accordingly (cf. Eq. (3)). Conversely, the coolant pump flow rate is mostly allocated on the lower end of the operating range, increasing only at points of maximum heating power demand (cf. Fig. 5a). This solution reflects the optimal allocation tendency to minimize the actuator losses and, thus, minimize the overall energy consumption, as discussed in more detail in Section IV.

The obtained optimal control allocation dependencies (Figs. 5a, 5b and 5e) are directly implemented within the control strategy Fig. 2 as lookup tables (maps). Alternatively, the allocation maps could be approximated by analytical expressions relating the map outputs to inputs, as demonstrated in [6].

Robustness of the optimal allocation maps has also been verified with respect to key effects of HVAC system unmodeled dynamics, including: (i) variation of cabin-HVAC system recirculation air temperature T_{rec}, where $T_{rec} > T_{cab}$ holds due to the distributed nature of minibus cabin thermal model, and (ii) deviations in ambient temperature relative to the nominal condition $T_{amb} = 0\,°\text{C}$. To assess the influence of these effects, the allocation maps were reoptimized for $T_{rec} = T_{cab} + 5$, and $T_{amb} = \{-10, 10\}°\text{C}$, and the results were compared with those obtained under the nominal scenario ($T_{rec} = T_{cab}$, $T_{amb} = 0°\text{C}$). Only minor differences in the total energy consumption have been observed across these cases, indicating good robustness of the proposed allocation approach to operational conditions uncertainties.

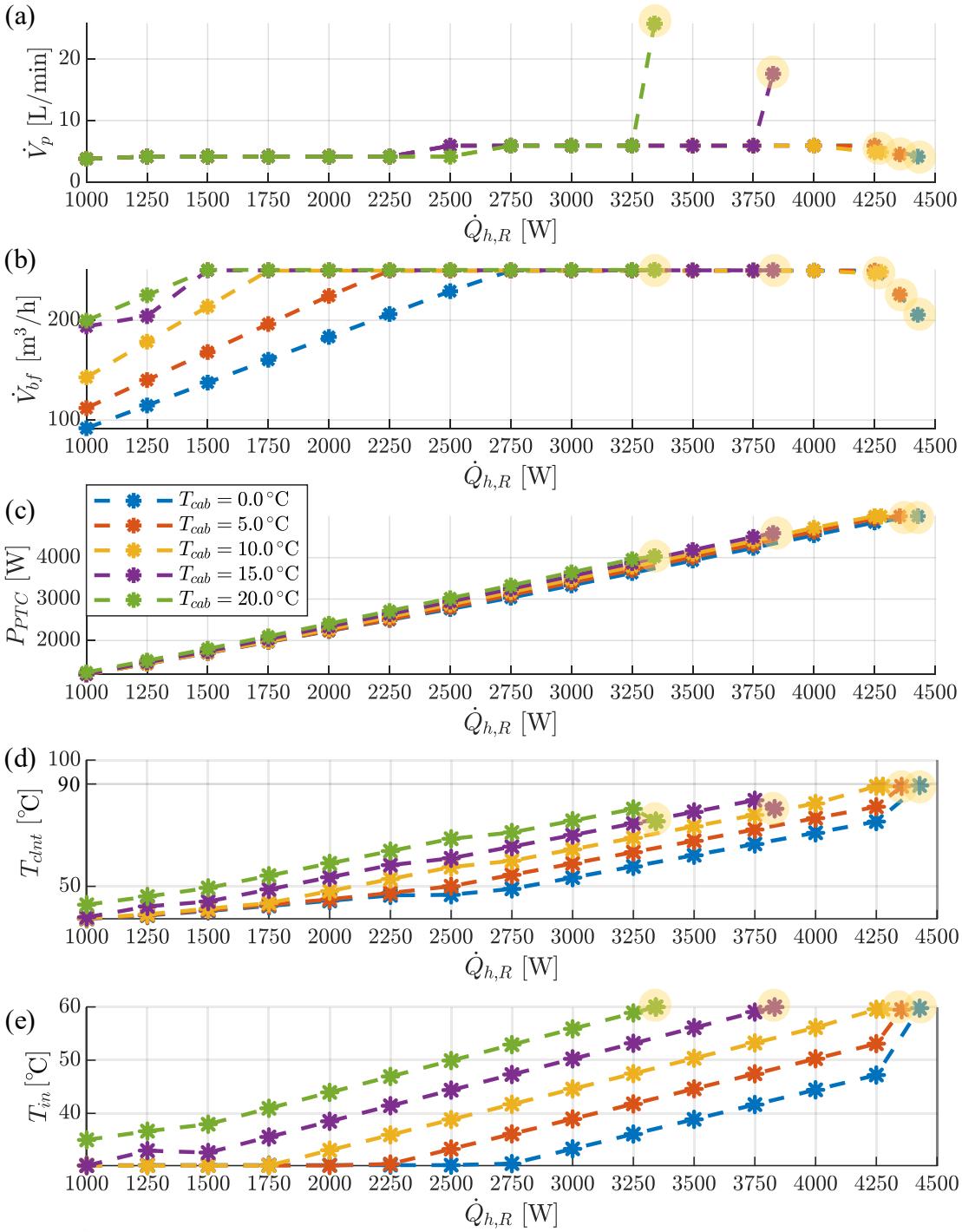

Figure 4. Optimal allocation maps

Low-level control

HVAC system model. The low-level PI controller should provide accurate tracking of cabin air inlet temperature and effective disturbance rejection (e.g., when changing the pump flow). For the sake of analytical controller parameter optimization, the HVAC model is represented by a linear second-order lag term extended with a pure delay term associated with coolant transport pipe length:

$$G_p(s) = \frac{T_{in}(s)}{P_{PTC,R}(s)} = \frac{K_{P1}}{(\tau_{P1}s + 1)(\tau_{P2}s + 1)} e^{-\tau_d s}. \quad (4)$$

The slow time constant (τ_{P1}) of the model (4) corresponds to heat transfer from the PTC heater into the coolant and depends strongly on the air blower fan flow $\dot{V}_{bf}$ (*PTC heater model* in Fig. 5). On the other side, the fast time constant (τ_{P2}) corresponds to heat transfer from the coolant fluid to the inlet air via the heater core and is primarily influenced by the coolant pump flow $\dot{V}_p$ (*Coolant to air heat exchanger* in Fig. 5).

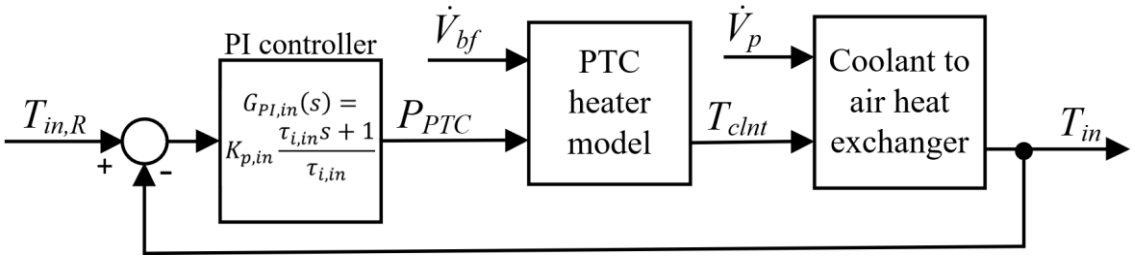

Figure 5. Structural block diagram of cabin inlet air low-level control loop

Identified numerical values of the time constants and the gain of transfer function (5) are shown in Fig. 7 for different operating points used in the previous section for optimization of the control allocation maps (cf. Table 1). The time constants are obtained by using the *tfest(.)* Matlab function and system responses with respect to step response of P_{PTC} input with an amplitude of approximately 5% of the maximum PTC power (a small-signal operating mode to which the linear model applies). The corresponding correlation indices, shown in the same figure, indicate that the slow time constat τ_{P1} and the system gain K_{P1} are strongly correlated with the blower flow ($r = -0.96$ on the scale from 0 to ∓ 1), while the fast time constant τ_{P2} correlates well with the pump flow ($r = -0.69$). The pure delay τ_d primarily depends on the coolant pump flow, and it ranges from approximately 3 to 4.5 s with the correlation coefficient $r = -0.71$.

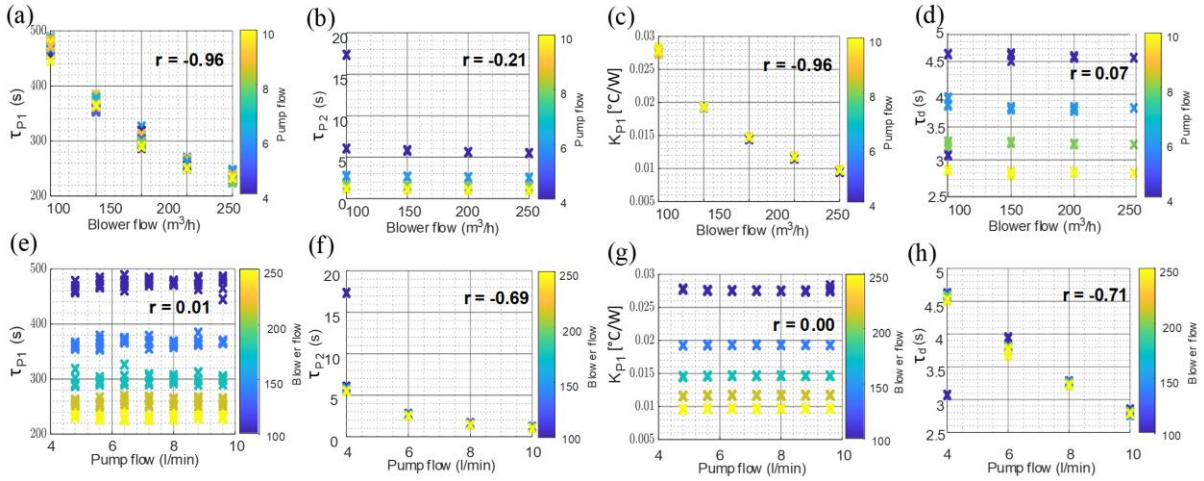

Figure 6. Identified parameters of process in low-level control system and respective correlation coefficients

One may assume that owing to a strong control effort, the closed-loop system would be much faster than the open-loop response dominated by the slow time constant τ_{P1}. Consequently, the second-order lag term may be simplified to a series connection of integral and first-order lag term, for which the analytical optimal solution for PI controller parameters exists (symmetrical optimum, [15, 16]):

$$G_p{}'(s) = \frac{T_{in}(s)}{P_{PTC}(s)} = \frac{K_P}{(\tau_{P1}s+1)(\tau_{P2}s+1)}e^{-\tau_d s} \approx \frac{K_P/\tau_{P1}}{s(\tau_{P2}{}'s+1)} = \frac{K_P{}'}{s(\tau_{P2}{}'s+1)} \qquad (5)$$

where the equivalent lag time constant τ'_{P2} also accounts for pure delay τ_d ($\tau'_{P2} = \tau_{P2} + \tau_d$ [15]). It is conservatively set on the upper edge of identified values ($\tau'_{P2} = 10\text{s}$) from Fig. 6. Another advantage of the process model simplification is that the integral gain $K'_P = K_P/\tau_{P1}$ is found to be rather independent of the process operating point (unlike the individual parameters K_P and τ_{P1}, see Fig. 6), thus avoiding the need for controller adaptation (i.e., gain scheduling).

Controller tuning and verification. The symmetrical optimum solution of the PI control controller parameters for the simplified process model given by Eqs. (6) is [16]:

$$K_{p,in} = \frac{2}{K_P{}'\tau_e}, \tag{6a}$$

$$\tau_{i,in} = \tau_e, \tag{6b}$$

$$\tau_{P1}/\kappa = \tau_{e,\max} \geq \tau_e \geq \tau_{e,\min} = 4\tau'_{P2}. \tag{6c}$$

The solution provides a well-damped (so-called quasi-aperiodic response), with the fastest (theoretically optimal) response obtained for the equivalent closed-loop system time constant τ_e set to $\tau_{e,\min}$. However, to reduce the control effort/energy and sensitivity to noise and process unmodelled dynamics, one may arbitrarily increase τ_e up to $\tau_{e,\max}$, which should be distant enough from the slow process time constant ($\kappa \cong 5$) to satisfy the assumption on integral+lag process dynamics description (6).

Here, the equivalent time constant is set to $\tau_e = 40$ s. The corresponding responses of the low-level closed-loop system involving the high-fidelity HVAC system model are shown in Fig. 7 for different coolant pump speeds, air blower flows and cabin temperatures. The small-signal operating mode responses are fast and well-damped for different operating points (see the detail of the response shown in the right-hand side column of Fig. 7). The fast response (much faster than the open-loop response) is owing to a strong control effort related to selection of fast equivalent time constant $\tau_e << \tau_{P1}$. The first part of the response in Fig. 8 (up to 700 s) indicate that the system behaviour is favourable in the large-signal operating mode, as well. Here, the response time is dictated by the PTC heater power-limit (set to 5000 W) and the operating point, and the responses remain well-damped.

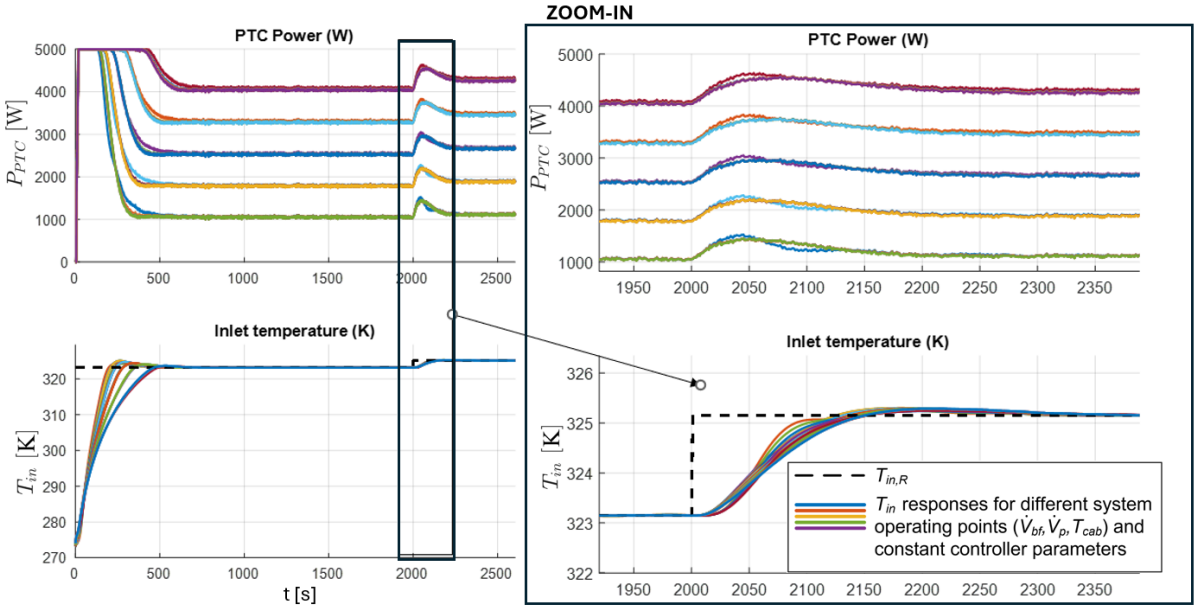

Figure 7. Responses of the low-level closed-loop system involving high-fidelity process model in different operating points

Coolant temperature safety mechanism. The PI controller of cabin air inlet temperature T_{in} cannot guarantee that the upper limit (3) of the coolant temperature T_{clnt} would be met. Namely, although the optimal allocation accounts for the constraint (3), in the large-signal operating mode transients the coolant temperature could exceed its limit. A potential solution could be to incorporate an inner controller of coolant temperature, but such a cascade control system would be more complex to tune and generally slower than the single-level controller one. Therefore, a simpler safety mechanism is proposed in Fig. 2, increases the pump flow in proportion to coolant temperature excess $T_{clnt} - T_{clnt,th}$, where the threshold $T_{clnt,th}$ is conservatively set somewhat below the temperature limit of 90 °C (to 85 °C, herein):

$$\Delta\dot{V}_{p,comp} = \begin{cases} K_{comp}\left(T_{clnt} - T_{clnt,th}\right), & \text{for } T_{clnt} > T_{clnt,th} \\ 0, & \text{for } T_{clnt} \le T_{clnt,th} \end{cases}. \tag{7}$$

As a result, the coolant temperature remains within the safe limits, as demonstrated by simulation results in Fig. 10e.

Superimposed cabin air temperature control

Process identification. The process in the superimposed cabin air temperature control loop, including both the control volume cabin model and the low-level control system, is identified by using the output-error (OE) discrete-time model defined in the z-domain as:

$$\begin{gathered} y(z) = z^{-n_k}\frac{B(z)}{F(z)}u(z) + e(z), \\ F(z) = 1 + f_1 z^{-1} + \cdots + f_{n_f} z^{-n_f},\ B(z) = b_0 + b_1 z^{-1} + \cdots + b_{n_b} z^{-n_b}, \end{gathered} \tag{8}$$

where $y = T_{cab}$ and $u = \dot{Q}_{h,R}$ are the process input and output, respectively (see Fig. 2), $B(z)$ and $F(z)$ are polynomials with free parameters to be identified, n_f and n_b are respective polynomial orders, n_k is the number of pure delay steps, and $e(z)$ is the output disturbance term accounting for measurement noise and unmodeled system dynamics.

The identification dataset is generated for multiple cabin temperature operating points, in which the system is excited by a chirp-type signal u covering a broad band of frequencies and having

the amplitude of about 2.5% of maximum $\dot{Q}_{h,R}$ value for the linear/small-signal operating mode operation. The MATLAB system identification toolbox has been used to candidate the models of different orders and identify their parameters. The selected model is of seventh order: n_f=7, $n_b = 3$, and $n_k = 4$.

Variations of the linearized HVAC model parameters across the cabin temperatures in the range of interest (e.g., $T_{cab} \in [15, 20]$ °C) are found not to be significant. Therefore, the controller parameters are fixed to those optimized for a single cabin temperature operating point: $T_{cab} = 17$ °C.

Controller parameter optimization. A modified PI controller is used, where the proportional (P) term is relocated into the feedback path to reduce the step response overshoot. The controller parameters K_p and τ_i are determined through numerical optimization [17] based following cost function is defined to minimize the closed-loop control error, as well as the control effort:

$$\min_{K_p,\,\tau_i} J_{11} = \sum_{k=1}^{N_w} H(k-W)\left(\left(T_{cab,R}(k) - T_{cab}(k)\right)^2 + r\left(\frac{\dot{Q}_{hR}(k)}{\dot{Q}_{hR,s}} - 1\right)^2\right), \qquad (9)$$

where k is the sampling step (note that the sampling time is set to 5 s, giving the sampling instants $t_k = kT$), r is the weighting coefficient that sets the trade-off between the two criteria, $H(k)$ is the Heaviside function defined by (10), and W is the number of initial sampling steps for which the cost function is not evaluated (due to inevitably high control error in the initial period).

$$H(k) = \begin{cases} 1, & \text{for } k \geq 0, \\ 0, & \text{for } k < 0. \end{cases} \qquad (10)$$

The control error and controlled variables $T_{cab,R} - T_{cab}$ and $\dot{Q}_{hR}$, respectively, are obtained as step responses of the closed-loop system comprising the discrete-time transfer functions of controller and identified process. The optimization is conducted through a search algorithm implemented through Matlab function *fminsearch*(.).

In the first optimization run, both W and r are set to 0 to emphasize the response speed criterion. Then, the initial/masking time window W is set to correspond to rise time of the first-run cabin temperature step response (H = 21), resulting in damping of the response, while the weighting coefficient r is adjusted to damp the residual response oscillations ($r = 0.05$).

Simulation results. Fig. 8 shows the cabin air temperature responses with respect to reference steps of 1 °C and 2 °C, where the overall control strategy from Fig. 2 is involved and both high-fidelity and identified linear process models are considered. In the small-signal operating mode (i.e., for the reference step of 1 °C), the responses of the systems with the high-fidelity and linear models are very similar to each other (see Figs. 8a and 8e). In contrast, for the higher reference step (2 °C), the response corresponding to the high-fidelity model deviates from the linear behaviour. This deviation primarily occurs because the inlet air temperature and pump flow reach saturation limits (see Figs. 8c and 8f). In the reference step-up case, the system response slows down as a result of saturation, but it remains stable and well damped. On the other hand, in the reference step-down case, the control input response reaches the lower saturation limit (Fig. 8e; this limit is related to the lower limit of T_{in} in Eq. (3)), which significantly disturbs the coolant pump and air blower fan flow allocation (see the blue lines in Figs. 8d and 8f). This is because the allocation was optimized for (quasi-)stationary conditions, and not for the abrupt transient occurring in this particular scenario. To make the operating conditions less abrupt for better allocation conditioning, a cabin temperature reference rate limiter is implemented in the direction of reference decrease. The reference decrease rate limit

is set as a trade-off of response speed and damping (-0.05 °C/s, herein). The corresponding response in Fig. 8 (solid orange line) indicates that applying the reference rate limiter significantly settles down the allocation responses and consequently dampens the cabin temperature and the heating power responses, without scarifying the response settling time.

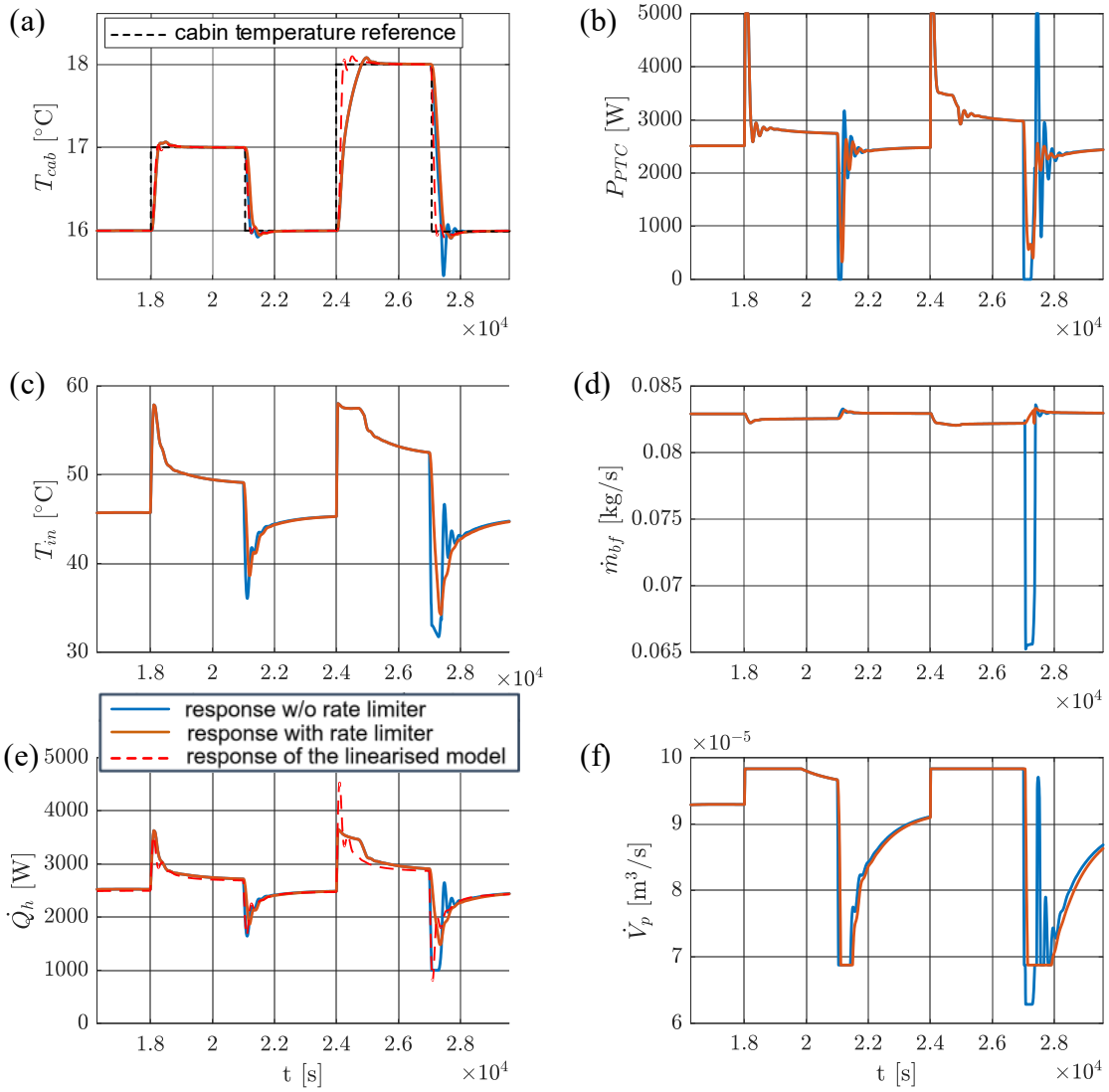

Figure 8. Step responses of overall hierarchical control strategy nonlinear (high-fidelity) and identified linear process models

VERIFICATION AGAINST INDUSTRY BASELINE

The proposed control strategy has been verified against the one reconstructed from real minibus data and experimental responses (denoted here as industry baseline), where both strategies are linked to the same high-fidelity HVAC system model. The baseline strategy employs a PI controller for regulating the coolant temperature at the fixed value of 75 °C, while the pump speed and the blower flows are set on fixed values of 250 m^3/h and 18 L/min. In the comparative verification study, the cabin temperature is not feedback controlled, i.e. the cabin thermal system operates in an open loop mode. The verification relates to both stationary and highly transient (heat-up) conditions.

Stationary conditions

The stationary conditions verification of the two strategies is based on the steady-state operating points used in the design of allocation maps (no cabin thermal model is involved). The results are shown in Fig. 9.

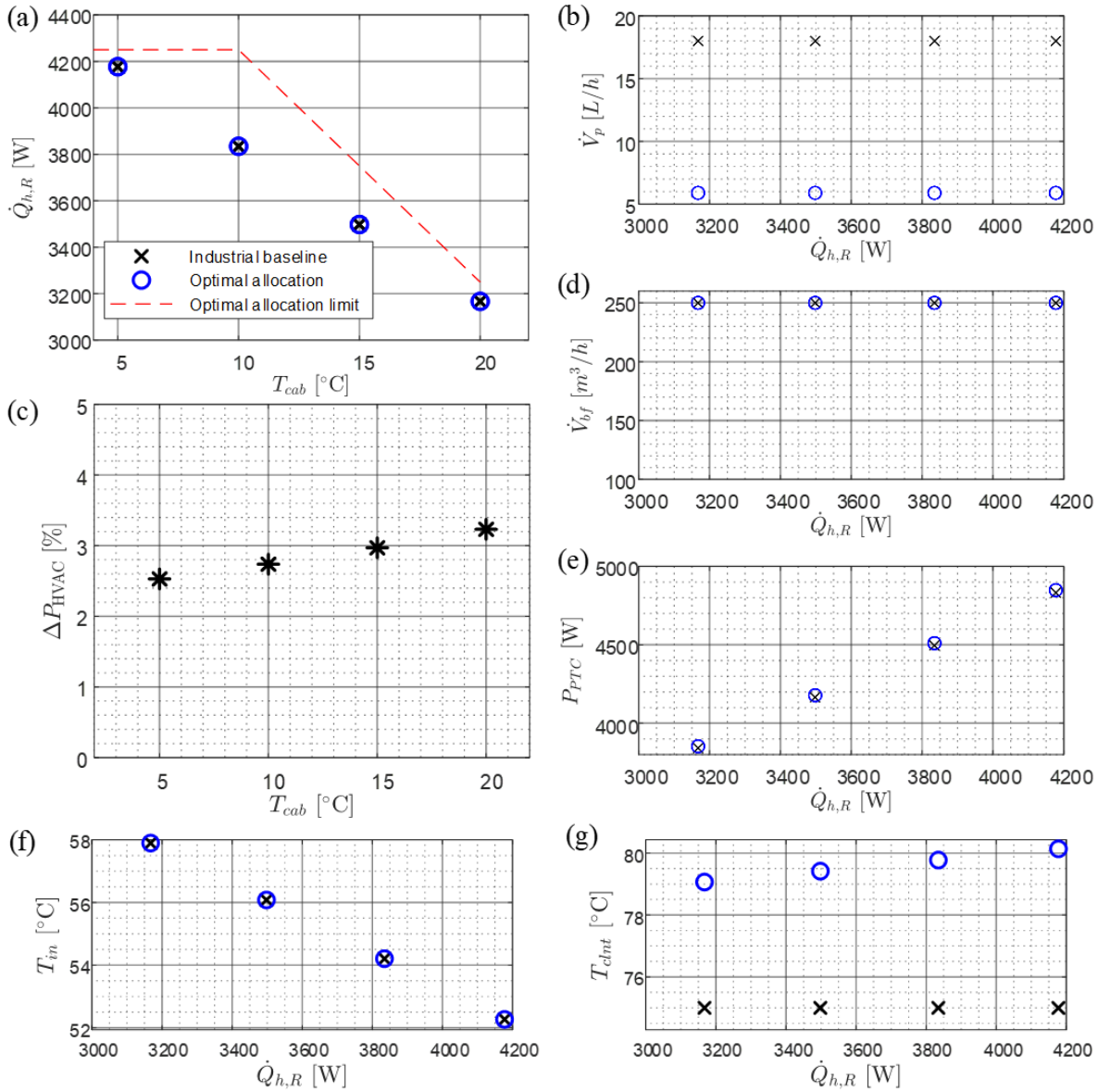

Figure 9. Comparative assessment of optimal allocation and industry baseline control strategies for stationary conditions

For equal $\dot{Q}_h$ at T_{cab} operating points, (see Fig. 9a), the control allocation (CA) strategy yields the power consumption savings in the range from 2.5% to 3.2% when compared to the baseline strategy (Fig. 9c). Comparing the allocations of $\dot{V}_p, \dot{V}_{bf}$ and P_{PTC} in Figs. 9b, 9d and 9e indicates that the savings predominantly comes from significantly reduced pump flow and a somewhat increased PTC power. The air blower fan flow setpoint remains at its maximum for both strategies. This maximum setting is justified by the relatively small blower unit with low associated losses. Operating below this level would result in an increased coolant temperature at the heater core outlet, with corresponding increased energy losses through the coolant circulation system.

To gain the insights in root causes of the power savings observed in Fig. 9, Table 2 compares the individual HVAC system power losses for the two control strategies, for the $T_{cab} = 20$ °C operating point, where $\dot{Q}_{h,loss}$ denotes thermal losses in the coolant circulation system, while $P_{p,loss}$ and $P_{bf,loss}$ denote the power losses in coolant pump and air blower fan. While the $P_{bf,loss}$ losses are expectedly equal in both cases (cf. Fig. 9d), a significant increase of the pump losses $P_{p,loss}$ is observed for the baseline vs. CA strategy which is due to the elevated level of the pump flow for the baseline strategy (Fig. 9b) and an exponential power loss dependency on the coolant pump flow. Conversely, reduced pump flows lead to coolant temperature increase (Fig. 9g), resulting in higher associated coolant thermal losses $\dot{Q}_{h,loss}$. However, the reduction in pump losses outweighs the increase in thermal losses, resulting in 19.8% total power loss decrease (Table 2) and, correspondingly, the total power consumption reduction of around 3%.

In addition to increased HVAC system energy efficiency, the CA strategy has potential to operate at higher heating power output than the industry baseline, as illustrated in Fig. 9a. This implies that the CA strategy not only operating more efficiently in (quasi-)stationary regime but can also reduce the heat-up response time (see next subsection). According to Fig. 9a, the maximum power boost of approximately 400 W occurs at around $T_{cab} = 10$ °C.

Table 2. Individual HVAC system power loses for CA case at ($T_{cab} = 20$ °C operating point from Fig. 9)

	$\dot{Q}_{h,loss}$ [W]	$P_{p,loss}$ [W]	$P_{bf,loss}$ [W]	Σ
Industry baseline	674.5 (0.0%)	156.9 (0.0%)	93.25 (0.0%)	988.4 (0.0%)
CA	686.8 (1.8%)	12.4 (-92.1%)	93.25 (0.0%)	792.4 (-19.8%)

Heat-up conditions

The two strategies are further compared for the highly transient, heat-up scenario, where the high-fidelity model includes the cabin thermal model in addition to the HVAC model. To match the open-loop temperature control in the baseline strategy, the CA strategy is operated along the HVAC heating power limits, as showed on Fig. 3. The comparative time responses are shown in Fig. 10 for several variants of CA strategy while the corresponding numerical results are presented in Table 1. The label CA denotes the case of CA strategy operating in the optimal, energy-efficient mode (see circles in Fig. 9a) corresponding to the nominal PTC power limit of 5000 W. The case designated by the label CA MAX corresponds to the same, nominal PTC power limit, but allows for the maximum heat power limit denoted by the red line in Fig. 3. The label PTC Boost denotes the scenario that exploits the short-term ability of PTC heater to exceed its power output up to 3000 kW (a feature present in the baseline strategy, see Fig 10b). For a fair comparison of the two strategies under the PTC boost conditions, the CA strategy is adjusted through a ramp-down limit of the low-level controller to resemble the baseline strategy response characterized by a relatively early and approximately linear fall of the PTC power from the boost level to the regular operating region (see Fig. 10b).

Table 3 presents the performance metrics for the different control strategies, and for the intervals of first 600 s of the heat-up phase and the full simulation interval of 9300 s (the latter corresponds to the interval on which the measurements were originally recorded [14]). For the shorter time horizon of 600 s, the cabin temperature T_{cab} rises to only around 7 °C from the initial temperature set to the ambient temperature T_{amb}= 0 °C (Fig. 10a). While the cabin temperatures of different strategies appear to be rather comparable (Fig. 10a), the main

differences can be observed in the cabin inlet air temperature responses (Fig. 10c), where the nominal CA strategy shows around 8% increase compared to the baseline strategy (see T_{in} column of Table 3), while the other CA strategies demonstrate even bigger increase (up to around 20%). The main root cause for this improvement is exploiting a wider range of coolant temperatures (up to the declared limit of 90 ºC, see Fig. 10e), and consequently keeping the PTC power at higher values once the initial boost phase ends (Fig. 10b). Consequently, the energy-efficient CA extended with the PTC boost option reaches the cabin temperature which is by around 7% higher than that of the baseline strategy (utilizing the PTC boost, as well). This is paid by the higher energy consumption E_{HVAC} (by the comparable margin of 7%).

Table 3. Comparison of performance indicators of different variants of control allocation strategy and industry baseline strategy for heat-up scenario

Ctrl. strategy	Results at t = 600s				Results at t = 9300s			
	T_{cab} [°C]	T_{in} [°C]	E_{HVAC} [kWh]	Q_{HVAC} [kWh]	T_{cab} [°C]	$T_{clnt,max}$ [°C]	E_{HVAC} [kWh]	Q_{HVAC} [kWh]
Industry baseline	7.50 (0.0%)	50.5 (0.0%)	0.892 (0.0%)	0.514 (0.0%)	19.35 (0.0%)	75.28 (0.0%)	10.353 (0.0%)	8.982 (0.0%)
CA	7.29 (−2.76%)	54.61 (8.14%)	0.851 (−4.72%)	0.472 (−8.29%)	19.16 (-0.98%)	84.48 (12.22%)	9.995 (−3.46%)	8.961 (−0.23%)
CA + PTC boost	8.01 (6.89%)	57.014 (12.90%)	0.954 (6.80%)	0.552 (7.32%)	19.17 (-0.93%)	84.6 (12.38%)	10.074 (−2.72%)	9.026 (0.40%)
CA max. limits	6.40 (−14.56%)	58.05 (14.96%)	6.383 (−5.24%)	5.497 (−12.11%)	19.47 (0.6%)	85.75 (13.91%)	10.526 (1.64%)	9.083 (1.03%)
CA max. limits + PTC boost	7.26 (−3.15%)	59.79 (18.40%)	6.402 (6.10%)	5.503 (3.45%)	19.49 (0.72%)	86.18 (14.48%)	10.609 (1.68%)	9.141 (1.68%)

*E_{HVAC} - HVAC system energy consumption, *Q_{HVAC} – HVAC system heat output, *$T_{clnt,max}$ – maximum achieved coolant temperature

However, over the full heat-up horizon (9300 s), the energy-efficient strategy achieves the energy consumption reduction of around 3% (somewhat higher if the PTC boost option is switched off), while the reached cabin temperature is only slightly lower (around 1%). The observed energy saving is consistent with the stationary results from Fig. 9c, with the note that the full heat-up response includes a dominant quasi-stationary (settling) temperature transient phase (see Fig. 10a, with the note that the settling phase is even longer for the full interval of 9300 s considered in the Table 3).

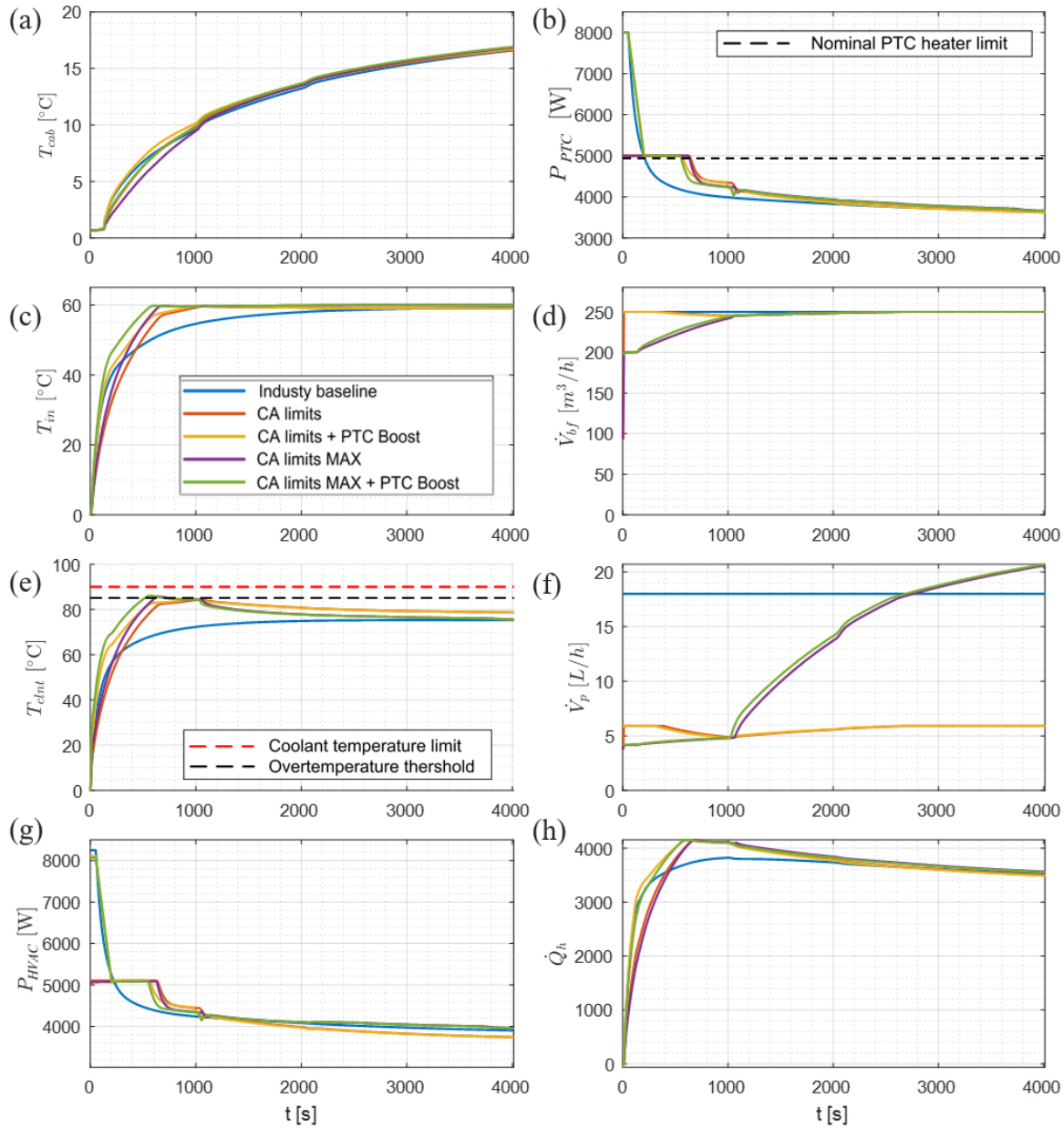

Figure 10. Comparative responses of control systems with different variants of control allocation strategy and industry baseline strategy for heat-up scenario

CONCLUSION

A hierarchical control allocation strategy has been proposed to effectively coordinate multiple, redundant actuators of a positive temperature coefficient (PTC) heater-based HVAC system of an electric minibus. The control framework also integrates a superimposed passenger cabin air temperature PI controller and a low-level cabin inlet air temperature PI controller, optimized for fast and well-damped responses. The former comprises reference rate and variable output limiters, while the latter is accompanied by a limiter of coolant temperature.

The overall control system has been verified through computer simulations for small- and high-signal operating modes based on an experimentally validated vehicle model consisting of high-fidelity HVAC and multi-zonal cabin models. When compared with an industry baseline strategy reconstructed from vehicle data and experimental responses, the proposed control strategy achieves the battery energy savings of approximately 3% under steady-state conditions,

which is owing to optimal control allocation. Similar, energy savings have been observed in the transient, heat-up scenario, with a minor effect on the response speed.

The future work will be directed towards modifying the allocation system for more effective behaviour in transient (heat-up) periods and designing a most-superimposed, thermal comfort control loop.

ACKNOWLEDGMENT

It is gratefully acknowledged that this paper has been produced as a part of research activity conducted through MINDED project (Thermal and energy Management for INcreased Driving range of an Electric minibus including improved user-centric Design and thermal comfort), which has received funding from the European Union's HORIZON EUROPE research and innovation programme under Grant agreement No. 101138202. The content of this publication is the sole responsibility of the MINDED consortium partners and does not necessarily represent the view of the European commission or its services.

REFERENCES

1. A. König, S. Mayer, L. Nicoletti, S. Tumphart, and M. Lienkamp, "The impact of HVAC on the development of autonomous and electric vehicle concepts, " *Energies*, Vol. 15, No. 2, 2022.
2. F. Fei and D. Wang, "PTC power control of electric vehicle thermal management system based on neural network feedforward," *Applied Thermal Engineering*, Vol. 253, No.1, 2024.
3. G. De Nunzio, A. Sciarretta, A. Steiner and A. Mladek, "Thermal management optimization of a heat-pump-based HVAC system for cabin conditioning in electric vehicles," *2018 Thirteenth International Conference on Ecological Vehicles and Renewable Energies (EVER)*, Monte Carlo, Monaco, 2018.
4. I. Cvok, B. Škugor, and J. Deur, "Control trajectory optimisation and optimal control of an electric vehicle HVAC system for favourable efficiency and thermal comfort," *Optimization and Engineering*, Vol. 22, 2021.
5. H. Khayyam, A. Z. Kouzani, E. J. Hu, and S. Nahavandi, "Coordinated energy management of vehicle air conditioning system," *Applied Thermal Engineering*, Vol. 31, No. 5, 2011.
6. I. Cvok, I. Ratković, and J. Deur, "Optimisation of Control Input Allocation Maps for Electric Vehicle Heat Pump-based Cabin Heating Systems," *Energies*, Vol. 13, No. 19, 2020.
7. I. Cvok, I. Ratković, and J. Deur, "Multi-objective optimisation-based design of an electric vehicle cabin heating control system for improved thermal comfort and driving range," *Energies*, Vol. 14, No. 4, 2021.
8. I. Cvok and J. Deur, "Control Trajectory Optimization of Electric Vehicle Heat Pump-Based Cabin Heating System," SAE Technical Paper 2025-01-8144, 2025.
9. S. Schaut and O. Sawodny, "Thermal Management for the Cabin of a Battery Electric Vehicle Considering Passengers' Comfort," in *IEEE Transactions on Control Systems Technology*, Vol. 28, No. 4, 2020.

10. I. Cvok and J. Deur, "Nonlinear Model Predictive Control of Electric Vehicle Cabin Cooling System for Improved Thermal Comfort and Efficiency," *2022 European Control Conference (ECC)*, London, United Kingdom, 2022.
11. N. Zhang, Y. Lu, Z. H. Ouderji, and Z. Yu, "Review of heat pump integrated energy systems for future zero-emission vehicles," *Energy*, Vol. 273, 2023.
12. Z. Zhang, W. Li, J. Shi, and J. Chen, "A study on electric vehicle heat pump systems in cold climates," *Energies*, Vol. 9, No. 11, 2016.
13. H. Ji, J. Cai, J. Pei, X. He, F. Guo, and Y. Wang, "Research on Heat Pump PTC Coupling Heating Strategy for Electric Vehicle," *Automotive Engineering*, Vol. 44, No. 10, 2022.
14. T. Bäuml, I. Maric, D. Dvorak, D. Šimić, and J. Konrad, "Modelling and experimental validation of the heating system and the thermal cabin model of an electric minibus,"*20th Conference on Sustainable Development of Energy, Water and Environment Systems (SDEWES)*, Dubrovnik, Croatia, 2025.
15. W. Leonhard, *Control of Electrical Drives*, 3rd ed. Berlin, Germany: Springer, 2001.
16. J. Deur, D. Pavković, "Fundamentals of Electrical Drive Controls", *UNESCO Encyclopedia of Life Support Systems*, 2012.
17. R. Isermann, *Digital Control Systems*, Springer-Verlag, Berlin, Heidelberg, 1981. doi: 10.1007/978-3-662-02319-8.